Acta Oceanol. Sin., 2020, Vol. 39, No. 4, P. 42–56
https://doi.org/10.1007/s13131-020-1535-y
http://www.hyxb.org.cn
E-mail: hyxbe@263.net

Vertical variations in the bio-optical properties of seawater in the northern South China Sea during summer 2008

Guifen Wang[1]*, Wen Zhou[2], Zhantang Xu[2], Wenlong Xu[1], Yuezhong Yang[2], Wenxi Cao[2]

[1] College of Oceanography, Hohai University, Nanjing 210098, China

[2] State Key Laboratory of Tropical Oceanography, South China Sea Institute of Oceanology, Chinese Academy of Sciences, Guangzhou 510301, China

Received 28 January 2019; accepted 27 May 2019

Abstract

Vertical variability in the bio-optical properties of seawater in the northern South China Sea (NSCS) including inherent optical properties (IOPs) and chlorophyll *a* concentration (*Chl*) were studied on the basis of *in situ* data collected in summer 2008 using an absorption/attenuation spectrophotometer. An empirical model was developed to estimate *Chl* profiles based on the absorption line height at long wavelengths, with a relative root mean square error of 37.03%. Bio-optical properties exhibited large horizontal and vertical spatial variability. As influenced by coastal upwelling and the Zhujiang River (Pearl River) discharge, both IOPs and *Chl* exhibited high values in the surface waters of the inner shelf, which tended to decrease with distance offshore. Subsurface maximum layers of IOPs and *Chl* were observed in the middle and outer shelf regions, along with significantly higher values of attenuation coefficients beneath this layer that rapidly increased towards the bottom. In the open ocean, both IOPs and *Chl* exhibited consistent variability, with the subsurface maximum layer typically located at 34–84 m. Phytoplankton were found to be one of the major components in determining the vertical variability of bio-optical properties, with their vertical dynamics influenced by both physical forcing and light attenuation effects. The depth of the subsurface maximum layer was found to be closely related to the fluctuation of the oceanic thermocline and the depth of the euphotic zone, which also affected the total integrated biomass of the upper ocean. Typically high values of attenuation coefficients observed in the bottom waters of the continental shelf reflected the transport of particulate matter over the bottom boundary layer. Our results reveal large spatial differences in bio-optical profiles in response to complex marine ecodynamics in the NSCS. From the perspective of marine research, high-resolution optical measurements are clearly advantageous over conventional bottle sampling.

Key words: vertical distribution, phytoplankton, bio-optical properties, subsurface maximum layer, northern South China Sea

Citation: Wang Guifen, Zhou Wen, Xu Zhantang, Xu Wenlong, Yang Yuezhong, Cao Wenxi. 2020. Vertical variations in the bio-optical properties of seawater in the northern South China Sea during summer 2008. Acta Oceanologica Sinica, 39(4): 42–56, doi: 10.1007/s13131-020-1535-y

1 Introduction

Since the 1980s, ocean scientists have become increasingly aware of the importance of the biogeochemical state of the oceans in regulating the climate and its effects on the habitability of the planet (Buesseler, 2001). Physical forcing and coupling of physical and biological processes have been found to exert a great influence on biogeochemical cycles (Platt et al., 2005). Additionally, new technologies with high vertical- and spatial resolutions have generated better understandings of short-term shifts in ocean biogeochemistry and linkages between physical forcing, biological responses and chemical fluxes on different spatial scales (Dickey, 2001).

Bio-optical studies aim to characterize the biological and biogeochemical state of natural waters based on their optical properties, and to quantify the role of the ocean in the global carbon budget (Morel and Maritorena, 2001). Inherent optical properties (IOPs), including absorption, scattering, backscattering and attenuation coefficients could be used to obtain the information (such as the amount, type and composition) of suspended particles and colored dissolved organic matter (CDOM) (Mobley, 1994; Boss et al., 2007). With the development of new optical sensors and monitoring platforms, optical observations have played significant roles in studying the biogeochemical dynamics of the upper ocean (Morel, 1988; Morel and Maritorena, 2001; Boss et al., 2001; Behrenfeld and Boss, 2003; Platt et al., 2005; McGillicuddy, 2016). The introduction of new devices, such as the spectral absorption-attenuation meter (WETLabs ac9/acs) and the Spectral Backscattering Sensor (HOBILabs hs6), has permitted *in situ* measurements of IOPs, including spectral absorption/attenuation coefficients and backscattering coefficients, at high resolutions (Chang and Dickey, 2001; Oubelkheir and Sciandra, 2008; Boss et al., 2013; Brewin et al., 2016). Converting these

Foundation item: The National Natural Science Foundation of China under contract Nos 41776045 and 41576030; the Fundamental Research Funds for the Central Universities under contract No. 2017B06714; the Open Project Program of the State Key Laboratory of Tropical Oceanography under contract No. LTOZZ1602; the Science and Technology Program of Guangzhou, China under contract No. 201607020041.

*Corresponding author, E-mail: guifenwang@hhu.edu.cn

measured IOPs to meaningful biogeochemical quantities is therefore a promising approach for studying biogeochemical variability at the scale of these observations (Oubelkheir et al., 2005).

During the last two decades, many studies have focused on developing rapid, continuous, *in situ* techniques for retrieving information about biogeochemical constituents (e.g., phytoplankton, sediment and dissolved matter) based on their relationships with optical properties. For example, beam attenuation has been used as a proxy for particulate organic carbon (POC) in the open ocean (Bishop, 1999; Gardner et al., 1999), and chlorophyll fluorescence and absorption have been used as proxies for chlorophyll concentration (Boss et al., 2007; Cullen, 1982; Mignot et al., 2011; Roesler and Barnard, 2013; Lavigne et al., 2015). These optical data have improved our understanding of the vertical distributions of biogeochemical parameters (Boss et al., 2001; Chang and Dickey, 2001), the formation of subsurface phytoplankton biomass maxima (Fennel and Boss, 2003; Nencioli et al., 2010) and the diel and seasonal cycles of particulate organic matter (Oubelkheir and Sciandra, 2008; Gernez et al., 2011; Kheireddine and Antoine, 2014; Mignot et al., 2014). Optical properties are also thought to serve as a link between physical and biogeochemical processes, as changes in the underwater light field lead to changes in biological activity (Fujii et al., 2007; Xiu and Chai, 2014).

The South China Sea (SCS) is the largest tropical marginal sea in the world. It covers an area of 3.5×10^6 km^2, with a maximum depth of over 5 000 m. Strongly influenced by the Asian monsoon, the SCS is characterized by diverse spatial-, temporal-, physical- and biological dynamics which play an important role in regulating the biogeochemical state of the SCS on both the horizontal and vertical scales (Liu et al., 2002; Ning et al., 2004). Bio-optical properties including the chlorophyll *a* concentration (*Chl*), phytoplankton absorption and the light absorption of colored detrital materials in the surface ocean of the SCS have been widely used for studying the environmental effects of physical processes at large spatial and temporal scales (Ma et al., 2011; Shang et al., 2012; Liu et al., 2013; Pan et al., 2015). Phytoplankton has been found to be the major contributing component of variations in the bio-optical properties of SCS seawater (Lin et al., 2014; Wang et al., 2008). However, only a few studies have so far focused on determining the high resolution vertical-scale bio-optical properties of SCS seawater (e.g., Lin et al., 2014; Zhang et al., 2016; Cui et al., 2016; Xu et al., 2018). Recent discussion about the vertical distribution of phytoplankton is predominantly based on data obtained from samples collected at discrete depths in the SCS (Gong et al., 2015; Li et al., 2016; Wang et al., 2016, 2018). Previous studies have proposed that vertical mixing on the shelf is the primary mechanism for bringing nutrients from the subsurface of the adjoining northern SCS up to the mixed layer, thereby supporting primary production (Chen et al., 2006; Wong et al., 2015). In the northeastern SCS, an increasing role of turbulent diffusion from the coastal ocean zones to the offshore pelagic zones, but a decreasing role of curl-driven vertical transport of nutrients, has also been found to be an important factor controlling phytoplankton dynamics (Li et al., 2016). During the period of September 2014–August 2015, two Bio-Argo floats were successfully used to describe the vertical variability of *Chl* in the open SCS, demonstrating the invaluable advantages of this method for observing biogeochemical properties over long time periods (Zhang et al., 2016). High-resolution bio-optical profile data collected over the entire SCS region are needed to provide a better understanding of the vertical structure of biogeochemical properties in this region including the important driving mechanisms.

This paper presents high-resolution observations of vertical variations of IOPs and *Chl* across the shelf sea of the northern SCS (NSCS). These data enable us to examine variations of IOPs in NSCS seawater and to produce estimates of *Chl* based on collected absorption spectra and the ratio of *Chl* to $c_{pg}(650)$, which are used as an indices of phytoplankton abundance and particle composition, respectively. We also examine differences in the vertical distributions of bio-optical properties over the continental shelf and in the open ocean, and the response of these properties to various hydrographical characteristics. We likewise consider factors that influence the observed spatial differences in bio-optical profiles by considering physical drivers including complex hydrodynamic processes and variations in light attenuation.

2 Data and methods

2.1 *Study region*

Hydrographic, bio-optical, and biogeochemical data from the NSCS were simultaneously acquired during the Opening Research Cruise of the R/V *Shiyan 3*, operated by the South China Sea Institute of Oceanology, Chinese Academy of Sciences, from August 16 to September 6, 2008. Figure 1 shows a map of the investigated station locations. The NSCS shelf can be sub-divided into the inner shelf, the middle shelf and the outer shelf corresponding to water depths of <40 m, 40–90 m and 90–120 m, respectively (Wong et al., 2015). Open ocean generally refers to water depths greater than 120 m.

2.2 *Hydrographic data acquisition and process*

Vertical profiles of temperature and salinity were acquired using a ship-launched SeaBird CTD and sampling rosette. The ocean mixed layer is the top layer of the water column, where the temperature and salinity are vertically well mixed. The mixed layer depth (MLD) was defined using the threshold method with a finite difference criterion based on a near-surface reference value. The reference depth is set at 10 m to avoid much of the strong diurnal temperature cycle that occurs in the top few meters of the ocean. The chosen temperature criterion is 0.5°C absolute difference, as recommended by Kara et al. (2000).

2.3 *Measurements of in situ optical profiles*

In situ profiles of inherent optical properties (IOPs) were measured using a ship-deployed profiling package at 48 stations, as shown in Fig. 1. The WETLabs ac9, which consists of dual, 25 cm path length flow tubes for each path, was used to measure the spectral absorption and attenuation coefficients at nine wavelengths (412, 440, 488, 510, 532, 555, 650, 676 and 715 nm). The ac9 data were corrected for temperature- and salinity effects using the coefficients derived by Sullivan et al. (2006). The proportional method (Zaneveld et al., 1994) was the applied to correct for scattering errors in the absorption measurements. We did field calibration before and in the middle of the observation period to monitor the stability of the ac9. Here, $a_{pg}(\lambda)$ and $c_{pg}(\lambda)$ denote the non-water spectral absorption and attenuation coefficients, respectively. All notations are as shown in Table 1.

Apparent optical profile data were collected at about 16 stations during the daytime. A freefall spectroradiometer (Satlantic, Inc.) was used to measure the vertical profiles of downwelling spectral irradiance ($E_d(z, \lambda)$) and upwelling spectral radiance ($L_u(z, \lambda)$) at seven wavelengths (412, 443, 490, 520, 555, 620 and

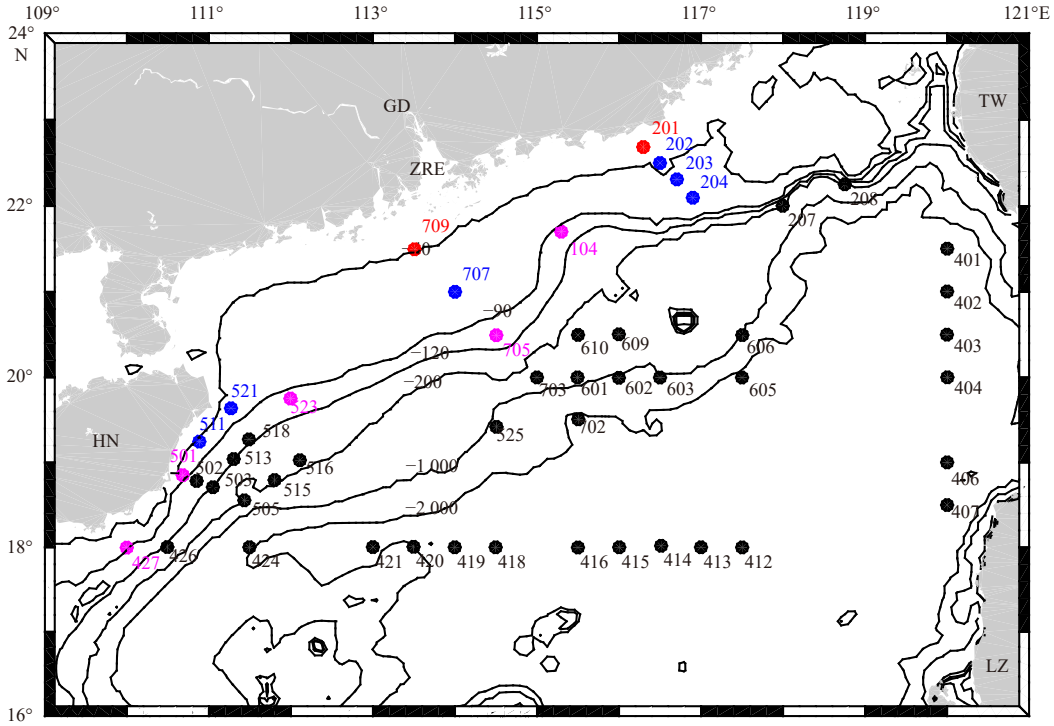

Fig. 1. Sampling stations in the northern South China Sea during the survey period of August 16–September 2, 2008. ● represents optical measurement station, ZRE Zhujiang River Estuary, GD Guangdong Province, TW Taiwan Island, LZ Luzon, and HN Hainan Island. Differently colored station labels refer to stations in different sub-regions: inner shelf (red), middle shelf (blue), outer shelf (magenta), and open ocean (black).

Table 1. Notations

Parameter	Value
λ	wavelength (nm)
$a_{pg}(\lambda)$	non-water absorption coefficient measured by the ac9 (m^{-1})
$a_p(\lambda)$	absorption coefficient of particle measured by spectrophotometer (m^{-1})
$a_{ph}(\lambda)$	absorption coefficient of phytoplankton measured by spectrophotometer (m^{-1})
$c_{pg}(\lambda)$	non-water attenuation coefficient measured by the ac9 (m^{-1})
$b_p(\lambda)$	scattering coefficient of particles measured by the ac9 (m^{-1})
$b_{bp}(\lambda)$	backscattering coefficient of particles measured by hs6 (m^{-1})
$a_{LH}(676)$	absorption line height at 676 nm (m^{-1})
Chl	chlorophyll *a* concentration (mg/m^3)
Chl_{surf}	surface chlorophyll *a* concentration (mg/m^3)
$<Chla>_{Zeu}$	integrated cholorophyll *a* biomass over the euphotic zone (mg/m^2)
POC	particulate organic carbon concentration (mg/m^3)
SCML	subsurface chlorophyll maximum layer
MLD	mixed layer depth (m)
Z_{eu}	euphotic zone depth (m)
Z_{SCM}	depth of the subsurface chlorophyll maximum layer (m^{-1})
Chl_{max}	magnitude of the subsurface chlorophyll maximum layer (mg/m^3)
T	temperature (°C)
S	salinity
θ	potential temperature (°C)
σ_θ	potential density (kg/m^3)
PAR	photosynthetic active radiation (quanta/(cm^2·s))

683 nm) away from the ship's shadow. Photosynthetic active radiation (PAR (quanta/(cm^2·s)) was calculated from $E_d(z, \lambda)$ spectra with the ProSoft software provided by Satlantic Inc. The depth of the euphotic zone, Z_{eu}, defined as the depth where irradiance was reduced to 1% of its surface value, was calculated based on the vertical profile of PAR.

2.4 *Collection and analysis of water samples*

Water samples were collected using Niskin bottles at selected depths (0 m, 10 m, 25 m, bottom in the coastal ocean, and 0 m, 25 m,

50 m, 100 m in the open ocean) to determine the *Chl*, the particulate absorption coefficient ($a_p(\lambda)$), and the particulate organic carbon (POC) concentration.

Water samples of roughly 0.5–1 L were collected at standard depths within the euphotic zone to be measured for *Chl*. Filters were flash-frozen and initially stored in liquid nitrogen and then stored at –80°C prior to analysis in the laboratory. Pigments were extracted with acetone at –20°C for about 24 h under dark conditions, and then analyzed with a Turner Designer 10 fluorometer (Parsons et al., 1984). Light absorption by suspended particles ($a_p(\lambda)$) was determined using the quantitative filter technique (QFT) (Mitchell et al., 2003; Lin et al., 2014). POC data were obtained using a method generally consistent with the Joint Global Ocean Flux Study (JGOFS) protocols (Knap et al., 1996; Wang et al., 2011).

2.5 *Remote sensing observations*

Daily sea level anomaly (SLA) data, based on a merged product from multiple satellite missions (T/P and ERS-1/2, followed by Jason-1/2 and Envisat) and distributed by Archiving, Validation and Interpretation of Satellite Oceanographic data (AVISO, http://www.aviso.oceanobs.com/) were used to describe the background physical properties of the seawater. These have been mapped to global Mercator grids with (1/4)°×(1/4)° spatial resolution. Maps of sea surface temperature (SST) with a 6 km×6 km spatial resolution were provided by the Group for High-Resolution Sea Surface Temperature (GHRSST) Project. Daily satellite chlorophyll data were collected from version 3.0 of the Ocean Colour Climate Change Initiative (OC-CCI) and a merged MERIS, MODIS-Aqua, SeaWiFS and VIIRS products available at http://www.oceancolour.org/).

2.6 *Bulk variability of IOPs and estimation of Chl profiles*

2.6.1 *Variations of non-water absorption and attenuation coefficients*

Our observed non-water absorption coefficients ($a_{pg}(\lambda)$) and non-water attenuation ($c_{pg}(\lambda)$) exhibited large variations among both coastal and offshore waters. A reference wavelength of 488 nm was selected to compare these data in the SCS with published results from other locations (Barnard et al., 1998; Boss et al., 2013). The $a_{pg}(488)$ ranged from 0.003 5–0.264 8 m^{-1}, with an average value of 0.029 5 m^{-1} (standard deviation (STD) = 0.016 3 m^{-1}); about 93% of the data points are less than 0.05 m^{-1}. On average, the value of $c_{pg}(488)$ is 6.68 times the value of $a_{pg}(488)$. About 98% of the calculated $c_{pg}(488)$ values lie between 0.059–0.50 m^{-1}, with an average value of 0.196 m^{-1} (STD=0.192 m^{-1}).

By matching data collected at discrete depth intervals, we performed a linear regression of the logarithms of total non-water absorption at 488 and 676 nm with *Chl* (Fig. 2a). $a_{pg}(488)$ and $a_{pg}(676)$ are closely related to *Chl*, and their relationships can be effectively described by power law functions, with an R^2 of 0.716 and 0.712, respectively. In the main absorption wavelengths (488 nm and 676 nm), the non-water absorption coefficients ($a_{pg}(\lambda)$) measured by the ac9 were linearly correlated with the total particulate absorption coefficients (a_p) measured for discrete samples and by QFT, with R^2 values of 0.744 and 0.577, respectively (Fig. 2b). The relationship between $c_{pg}(488)$ and *Chl* can be described by a linear function, with an R^2 value of 0.60 (Fig. 2c). The correlation between $c_{pg}(650)$ and bottle measurements of POC was examined using a least-square linear regression, with an R^2 value of approximately 0.544 and the Relative Root Mean Square Error (denoted as RMSE, %) of approximately 43.4% (Fig. 2d). This relationship showed some difference from that developed by Stramski et al. (2008) for the eastern South Pacific and eastern

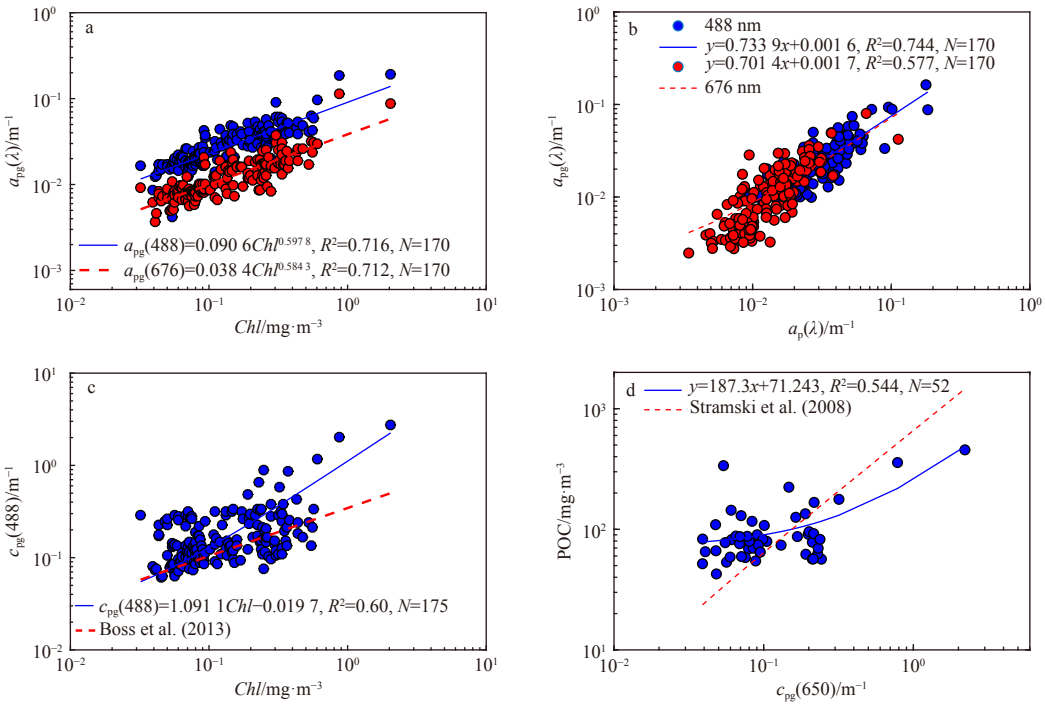

Fig. 2. Non-water absorption (a_{pg}) at 488 nm and 676 nm measured by ac9 vs. *Chl* (a), and their comparisons with total particulate absorption measured by the quantitative filter technique (b); non-water attenuation (c_{pg}) at 488 nm vs. *Chl* (c), and c_{pg} at 650 nm vs. particulate organic carbon (d).

Atlantic Ocean. Based on our data analysis, the POC in surface ocean was correlated with the *Chl*, with the R^2 being around 0.56 (N=50) for the power law relationship.

2.6.2 *Estimation of chlorophyll a concentration from absorption*

Different models have been developed to retrieve *Chl* from the absorption spectra. Since the pigment absorption peak in the red wavelength (676 nm) is primarily associated with chlorophyll *a*, we can obtain a proxy for *Chl* by regressing the power-law relationship between $a_{pg}(676)$ and *Chl*, as shown in Fig. 2a, with the RMSE of 42.56% and a log-transformed root mean square error (RMSE-log) of 0.170.

$$Chl = 33.377 a_{pg}(676)^{1.244}, \quad R^2 = 0.693, \ N = 168. \tag{1}$$

This empirical relationship is significantly different than that developed by Claustre et al. (2000), which might be due to a scattering offset in the absorption meter for longer wavelengths, as well as the absorption contribution of other pigments or colored detritus materials.

An alternative index is the difference between the absorption at 676 nm and that at 650 nm divided by the chlorophyll-specific absorption at 676 nm (0.014 m^2/mg) (Chang and Dickey, 2001; Fennel and Boss, 2003; Xiu et al., 2009), with the relationship being expressed mathematically by the following equation:

$$Chl = \frac{a_{pg}(676) - a_{pg}(650)}{0.014}. \tag{2}$$

This model (Eq. (2)) exhibited poor performance in our study area, with a RMSE of 85.46%, and a RMSE-log of 0.31. For certain samples, the $a_{pg}(650)$ was even higher than $a_{pg}(676)$, resulting in a negative value for *Chl*.

In recent years, some researchers have preferred to calculate the height of the peak absorption above a baseline drawn between the absorption at 650 nm and that at 715 nm (Boss et al., 2013; Roesler and Barnard, 2013) to approximate the phytoplankton absorption at 676 nm. The absorption line height ($a_{LH}(676)$) thus defined can be expressed as follows:

$$a_{LH}(676) = a_{pg}(676) - \left[\frac{39}{65}a_{pg}(650) + \frac{26}{65}a_{pg}(715)\right]. \tag{3}$$

The *Chl* can then be estimated from a linear correlation (Roesler and Barnard, 2013; Brewin et al., 2016) or a power-law relationship with $a_{LH}(676)$ (Boss et al., 2013). In this study, however, there was poor correlation between $a_{LH}(676)$ (estimated from Eq. (3)) and *Chl*, which might be related with the large variability of $a_{pg}(715)$ (–0.037 to 0.263 m^{-1}). We preferred to compute the absorption line height at 676 nm as $a_{pg}(676)$–0.6×$a_{pg}(650)$, and developed a power-law function for describing its relationship with *Chl*, as shown in Fig. 3a and Eq. (4), which exhibited a much high value of R^2 (0.77), with the RMSE and RMSE-log of 37.03% and 0.147, respectively.

$$Chl = 45.179\left[a_{pg}(676) - 0.6 \times a_{pg}(650)\right]^{1.139\,1}, \quad N = 168. \tag{4}$$

Unlike using the *in situ* fluorometric method to estimate chlorophyll, the absorption line height is not sensitive to the incident irradiance, in particular, the non-photochemical quenching that could promote initial chlorophyll fluorescence and result in an underestimation of *Chl* (Roesler and Barnard, 2013). A power-law function was recommended for describing the pigment packaging effect, which exhibited a robust relationship over the simple linear regression (Boss et al., 2013). By comparing the regional optimized model as shown by Eqs (1), (2) and (4), we can see that, by subtracting the absorption contribution by other components, the relationship between $a_{LH}(676)$ and *Chl* tends to converge. Therefore, this empirical algorithm (Eq. (4)) was used to estimate the vertical distribution of chlorophyll *a* based on the absorption profiles. According to frequency distribution of the 3 457 data points collected over 48 profiles (1 m interval) in the NSCS (Fig. 3b), our estimated *Chl* generally varies from 0.02 to 0.63 mg/m^3, with an average value of 0.161 mg/m^3.

2.6.3 *Definition and description of the subsurface chlorophyll maximum layer (SCML)*

Based on our estimated high-resolution chlorophyll profiles, we were able to calculate variations in the SCML, including thickness, depth (Z_{SCM}), and intensity (Chl_{max}). The thickness of the SCML can be estimated as the depth interval over which the *Chl* was 50% of the maximum *Chl* (Pérez et al., 2006; Gong et al., 2014). The deployed depth of the ac9 in some stations did not cover the whole profile of chlorophyll *a* (8 incomplete profiles out of 38). Therefore, the thickness of the SCML in our study was defined as 2×Δ*d*, where Δ*d* is the difference in depth between the location of Chl_{max} and *Chl*=50%Chl_{max} within the upper layer. The intensity of SCML (Chl_{max}) refers to the chlorophyll value at Z_{SCM}.

2.6.4 *Calculation of the integrated cholorophyll a biomass over the euphotic zone*

The integrated chlorophyll *a* biomass over the euphotic zone

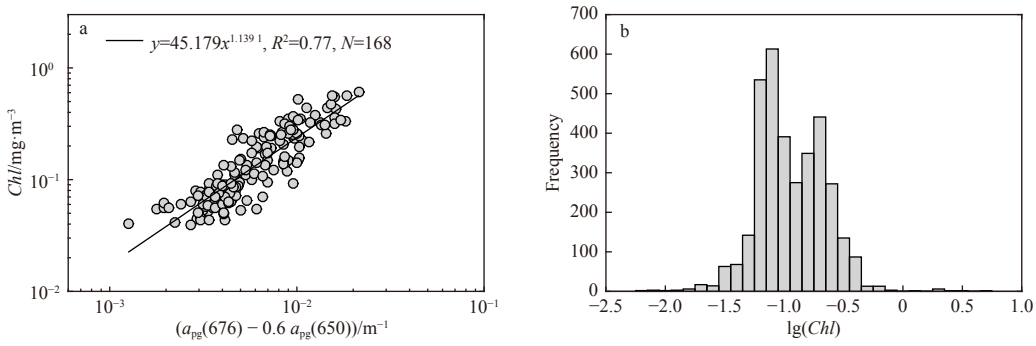

Fig. 3. Absorption difference ($a_{pg}(676)$–0.6×$a_{pg}(650)$) versus *Chl* (solid line represents the power-law function) (a), and frequency distribution of absorption-estimated *Chl* (b).

(<Chla>$_{Zeu}$) can be calculated from these *Chl* profiles. During the cruise, the depth of the bottom of the euphotic zone (Z_{eu}), which was measured at several stations, shows a clear relationship with the surface chlorophyll *a* concentration (Chl_{surf}) (Z_{eu}=26.767$Chl_{surf}^{-0.353}$, R^2=0.88, N=16). Thus, by using this modified bio-optical model, Z_{eu} can also be inferred from the surface value of *Chl*. Only the profiles where the bottom of the euphotic zone was reached are considered for such statistical analyses.

3 Results

3.1 *Hydrographic characteristics of the NSCS*

Following the classification of Wong et al. (2015), average hydrographic and IOPs in these hydrographic sub-divisions (inner shelf, middle shelf, outer shelf and the open ocean) in summer 2008 are summarized in Table 2. The relationship between potential temperature (θ, °C), and salinity (S) at observed stations across the shelf sea are shown in Fig. 4. The θ-S relationship in inner shelf waters is obviously different from that of the open ocean. Two stations collected in the inner shelf waters were located in a center of upwelling (with lower temperature and high salinity in the surface waters) and in the plume waters of the Zhujiang River Estuary (with high temperature and low salinity in the surface waters). In contrast, the water over the outer shelf was warm and saline, with a mean temperature of 28.7°C and a salinity of 33.56 in the mixed layer. The density of outer shelf water (mean σ_θ=21.10 kg/m^3) is even higher than that of the open ocean (σ_θ=20.82 kg/m^3). The middle shelf water was generally found to be a mixture of the inner- and outer shelf waters, with σ_θ=20.54 kg/m^3 and S=32.96. The extensions of θ-S relationships in the inner shelf converged with those further offshore at a salinity of roughly 34.2, a temperature of 22.03°C and a density of 23.74 kg/m^3. This point of convergence, which likely represents the source water of the inner shelf, was traced to a depth of about 40–50 m in the middle and outer shelf. Except for some specific points with low salinity in upper surface waters, the θ-S relationships in the outer shelf waters match well with those observed in the open ocean, which converged at a salinity of 34.5 and a temperature of 19.7°C.

Superimposed on these general hydrographic characteristics, coastal upwelling, river discharge in shelf waters, and meso-scale eddies in the open ocean are major additional sub-regional features in the study area. Intrusions of water from the Kuroshio Current, as well as the passage of typhoons, may also result in different vertical structures of hydrological properties. During the survey period (16 August–6 September 2008), the SST was generally high in most regions of the NSCS (>30°C), with the exception of two cold centers off the coast (Fig. 5a). One is located in the northeast part of the NSCS along the coast of Guangdong Province with the minimum value around 27.5°C, which is generally noted as the eastern Guangdong coastal upwelling (Wang et al., 2014). This upwelling event could also be detected in the SLA map, which displays significantly lower values in this region (Fig. 5b). The other cold center, which is relatively weaker (minimum SST = 29°C), appears to the northeast of Hainan Island, and is usually noted as the Hainan northeastern upwelling (Lin et al., 2016). Based on *in situ* data, obvious shoreward and upward tilting of the isotherms from the middle shelf to the inner shelf were observed in the eastern Guangdong coastal upwelling. The open ocean of the NSCS is mainly characterized by three anticyclonic eddies (ACE), detected by satellite sea level anomaly maps (SLA) (Fig. 5b). Two of them were located across the 18°N transect, with *in situ* sampling stations cutting through the centers of these ACEs. In the northeast part of SCS, there is another ACE across the Luzon Strait, with high SLA and high SST. Surface *Chl* exhibits obviously higher values along the coast of the NSCS (Fig. 5c), especially in the coastal upwelling regions and the Zhujiang River Estuary. In the offshore area, where water depth is greater than 120 m, *Chl* exhibits much lower values, with the spatial pattern largely matching that of SLA. Extremely low *Chl* values could be observed at the centers of identified ACEs. During the survey, the central part of the NSCS also exhibited high *Chl* as affected by the passage of typhoon Nuri (Ye et al., 2013).

3.2 *Vertical distributions of bio-optical properties in NSCS sub-regions*

3.2.1 *Inner shelf waters*

Two profiles were collected in the inner shelf region, at Stas 201 and 709 (Fig. 1). Station 201 lies near the center of coastal upwelling, with lower temperature and higher salinity present throughout the whole water column (Table 2, Fig. 6a). Station 201 also exhibited the highest values of IOPs and *Chl* (Fig. 7), in which the a_{pg}(488) and c_{pg}(650) were approximately 0.193 m^{-1} and 2.203 m^{-1}, respectively. Our absorption-estimated *Chl* for

Table 2. Average hydrographic properties and concentrations of chlorophyll *a* in the hydrographic sub-divisions in the northern South China Sea

Area	Inner shelf	Middle shelf	Outer shelf	Open ocean
Water depth/m	<40	40–90	90–120	>120
MLD/m		15–32	12–43	12–62
T/°C	24.43–29.58 (27)	27.83–29.82 (28.96)	28.06–29.47 (28.65)	27.64–29.75 (29.14)
S	31.53–33.41 (32.47)	32.08–33.68 (32.96)	33.41–33.70 (33.56)	33.05–33.66 (33.41)
σ_θ/kg·m^{-3}	19.27–22.31 (20.79)	20.22–20.82 (20.54)	20.86–21.29 (21.10)	20.56–21.48 (20.82)
a_{pg}(488)/m^{-1}	0.037–0.193 (0.115)	0.015–0.066 (0.029)	0.018–0.035 (0.025)	0.006–0.028 (0.017)
c_{pg}(650)/m^{-1}	0.111–2.203 (1.157)	0.072–0.507 (0.176)	0.067–0.237 (0.109)	0.04–0.224 (0.101)
Chl/mg·m^{-3}	0.207–2.109 (1.158)	0.066–0.382 (0.135)	0.086–0.143 (0.107)	0.022–0.113 (0.078)
Chl_{surf}[1)]/mg·m^{-3}	0.215–2.045 (1.13)	0.055–0.609 (0.182)	0.05–0.175 (0.090)	0.032–0.123 (0.067)
Z_{SCM}[2)]/m	9	25–56 (43)	34–50 (43.5)	34–84 (60.24)
Chl_{max}[2)]/mg·m^{-3}	5.139	0.243–0.811 (0.428)	0.437–0.490 (0.457)	0.184–0.481 (0.303)
<Chla>$_{Zeu}$[3)]/mg·m^{-2}	30.34	6.99–10.95 (9.34)	10.84–15.75 (13.11)	4.24–13.77 (8.17)
Thickness[2)]/m	3.8	4–44 (15.7)	12–26 (16.3)	7–54 (26.3)
Number of profiles	2	6	5	35

Note: [1)] *In situ* measured data at surface waters; [2)] only profiles with subsurface maximum layer of chlorophyll a are considered for statistics; [3)] only profiles where the euphotic depth are reached are considered for statistics.

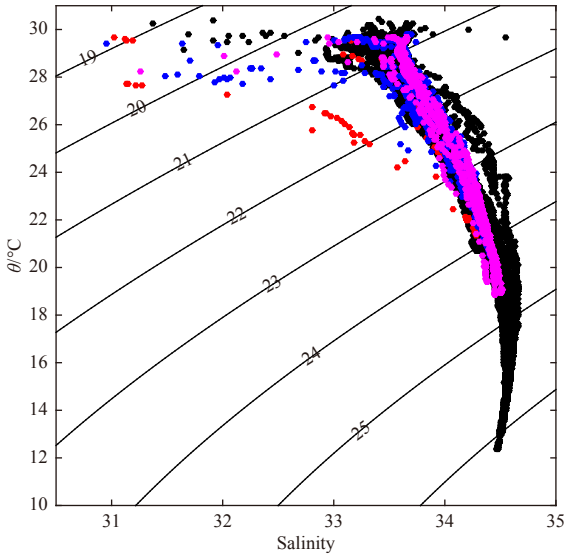

Fig. 4. The relationship between potential temperature (θ, °C) and salinity at each station observed in summer 2008 for stations from the inner shelf (red), middle shelf (blue), outer shelf (magenta), and open ocean (black). Lines of constant density (σ_θ, kg/m^3) are shown.

surface waters at Sta. 201 is 2.109 mg/m^3, which is similar to the results of *in situ* measured data (2.045 mg/m^3). An obvious SCML was observed at approximately 9 m with the thickness of about 3.8 m and Chl_{max} of up to 5.14 mg/m^3. Furthermore, the column-integrated biomass over the euphotic depth (<Chla>$_{Zeu}$) was up to 30.34 mg/m^2, indicating a strong contribution of coastal upwelling to phytoplankton growth. Both IOPs and *Chl*, as well as the ratio of *Chl* to $c_{pg}(650)$ ($Chl/c_{pg}(650)$), tend to decrease rapidly to a stable value below the SCM layer, which indicates the dominant role played by the scattering effect of particles in the bottom waters (Figs 7a and 8a).

The vertical distribution of bio-optical parameters at Sta. 709 is much different than that at Sta. 201. Station 709 lies in the mouth of Zhujiang River Estuary (Fig. 1). The upper surface water (about 4 m thick) was particularly fresh and the surface salinity dropped to as low as 31.53, which is about 2 lower than that of offshore waters (Fig. 6a). These characteristics were consistent with the influence of fresh water from the Zhujiang River. Both IOPs and our estimated *Chl* profiles exhibit high values in this upper layer compared with offshore stations (Fig. 7a). The vertical $a_{pg}(488)$ profile exhibits small peaks at approximately 16 m, and $c_{pg}(650)$ increases at depths below 21 m. There is no obvious peak in the vertical *Chl* profile and the average value over the water column is about 0.221 mg/m^3. The vertical profile of $Chl/c_{pg}(650)$ tends to at first increase and then decrease rapidly with the depth; the turning point for $Chl/c_{pg}(650)$ is at a depth of around 21 m (Fig. 8a).

3.2.2 *Middle shelf waters*

In the middle shelf, we collected six profiles: three in the eastern part of the Guangdong coastal area, two to the east of Hainan Island, and one at Sta. 707, offshore of the Zhujiang River Estuary (Fig. 1). Affected by coastal upwelling, surface water at Sta. 202 (as shown in Lin et al. (2014)) exhibits relatively lower temperature and higher IOPs and *Chl* than other stations (Fig. 6b). Elevated values of IOPs and *Chl* in the subsurface were observed at

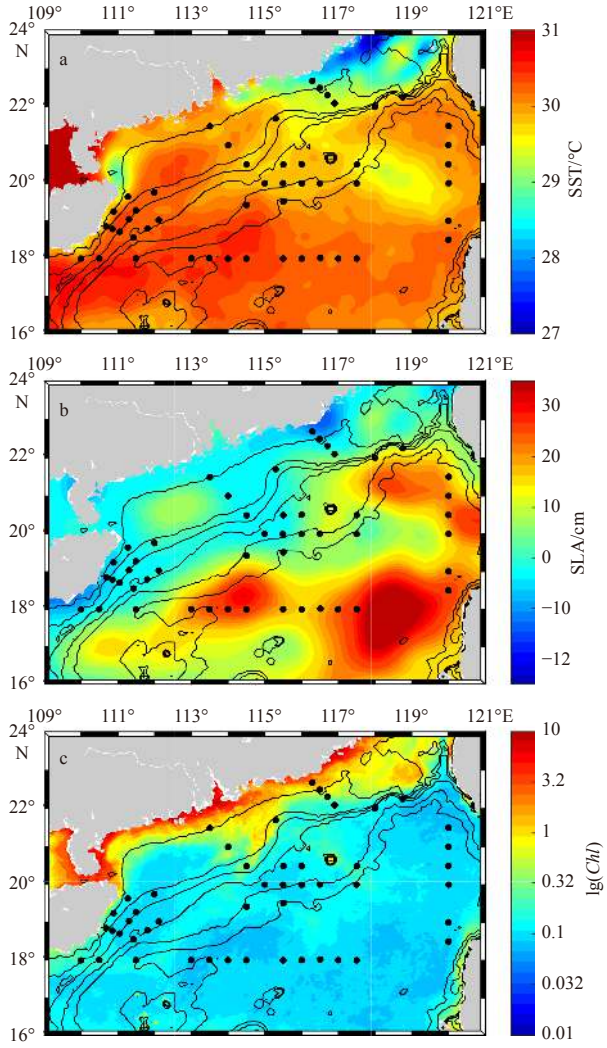

Fig. 5. The distribution of average sea surface temperature (SST, °C) (a), sea level anomaly (SLA, cm) (b), and surface chlorophyll *a* concentration (log-transformed) (c) in the NSCS during the summer 2008 survey period.

Sta. 511 along the coast of the Hainan Island, with a maximum *Chl* of 0.8 mg/m^3 (Fig. 7b). The location of Z_{SCM} varies from 25 m to 56 m, with the thickness of the SCML exhibiting a large variability from 4 m (202) to 44 m (521). Both IOPs and *Chl* are significantly lower than in inner shelf waters, but still higher than at outer shelf stations. <Chla>$_{Zeu}$ ranges from 6.99 mg/m^2 to 10.95 mg/m^2 exhibiting large spatial differences.

Another distinguishing characteristic of the vertical distribution of bio-optical properties in the middle shelf lies in the increasing trend of the attenuation coefficient towards the bottom below the Z_{SCM}. The particulate scattering coefficient provides a relatively large contribution to the light attenuation in the bottom waters. High concentrations of re-suspended particles are thought to be a major contributor to light attenuation, reflecting the transport of particulate matter across the shelf via the benthic nepheloid layer. Vertical plots of $Chl/c_{pg}(650)$ are generally characterized by constant values within the upper layer, gradually increasing to the depth of the SCML before rapidly decreasing toward the bottom (Fig. 8b).

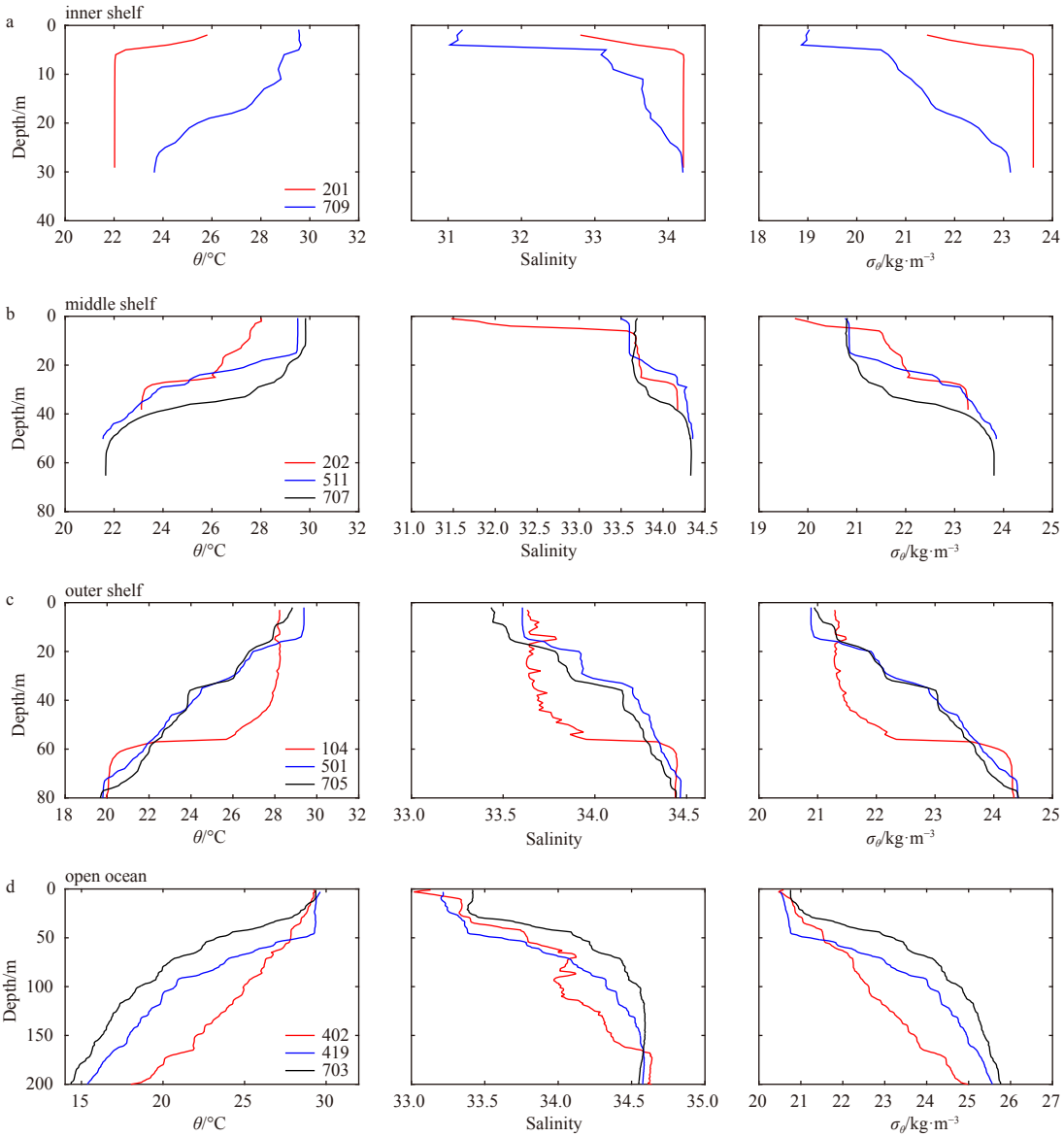

Fig. 6. Typical vertical distribution of potential temperature (θ, °C), salinity (S) and potential density (σ_θ, kg/m^3) at stations across the shelf of the NSCS: inner shelf (a), middle shelf (b), outer shelf (c), and open ocean (d).

3.2.3 *Outer shelf waters*

Outer shelf waters are obviously stratified, with the MLD ranging from 12 m to 43 m. For Stas 427 and 501, located around the Hainan Island, the thermoclines are relatively shallower than at other stations, with high values of $c_{pg}(650)$ observed in the bottom waters (Fig. 7c). Both the averaged hydrographical and bio-optical properties within the mixed layer are slightly higher than in middle shelf waters (Table 1, Figs 6c and 7c). The peaks of SCML are much more pronounced, with the Z_{SCM} varying from 34–50 m and an average thickness of roughly 16.3 m. The contribution of re-suspended particles in the bottom boundary layer to the light attenuation of re-suspended particles in the bottom boundary layer is relatively weak compared with waters in the middle shelf, and these also result in the gentle decrease of $Chl/c_{pg}(650)$ ratio below the depth of the SCML (Fig. 8c).

3.2.4 *Open ocean waters*

Open ocean waters over the ocean basin of the NSCS exhibit relatively high upper ocean temperatures and salinities (Fig. 6d). The average mixed layer depth (about 33.56 m) is deeper than that in the shelf waters (Table 1). Based on 35 vertical profiles measured *in situ*, bio-optical properties within the mixed layer are relatively lower than in the shelf waters. *Chl* within the mixed layer ranges from 0.022–0.113 mg/m^3, with an average value of 0.078 mg/m^3. Vertical profiles of IOPs and *Chl* are mainly characterized by a subsurface maximum, which occurs at similar depths and IOPs and *Chl* decrease in both the upward and downward directions away from the SCML. For most profiles in the open ocean, Z_{SCM} lies between 34–84 m and is deeper than the SCML observed in shelf waters. The average depth of Z_{SCM} is 60.24 m, though for some profiles, this depth is as much as 80 m. The magnitude of the SCML in open ocean water is significantly lower than that of shelf waters, with the values ranging from 0.184–0.481 mg/m^3 (average=0.303 mg/m^3). As estimated from the surface chlorophyll *a* concentration, the euphotic zone depth ranges from 60 m to 100 m, and the integrated $<Chla>_{Zeu}$ lies between

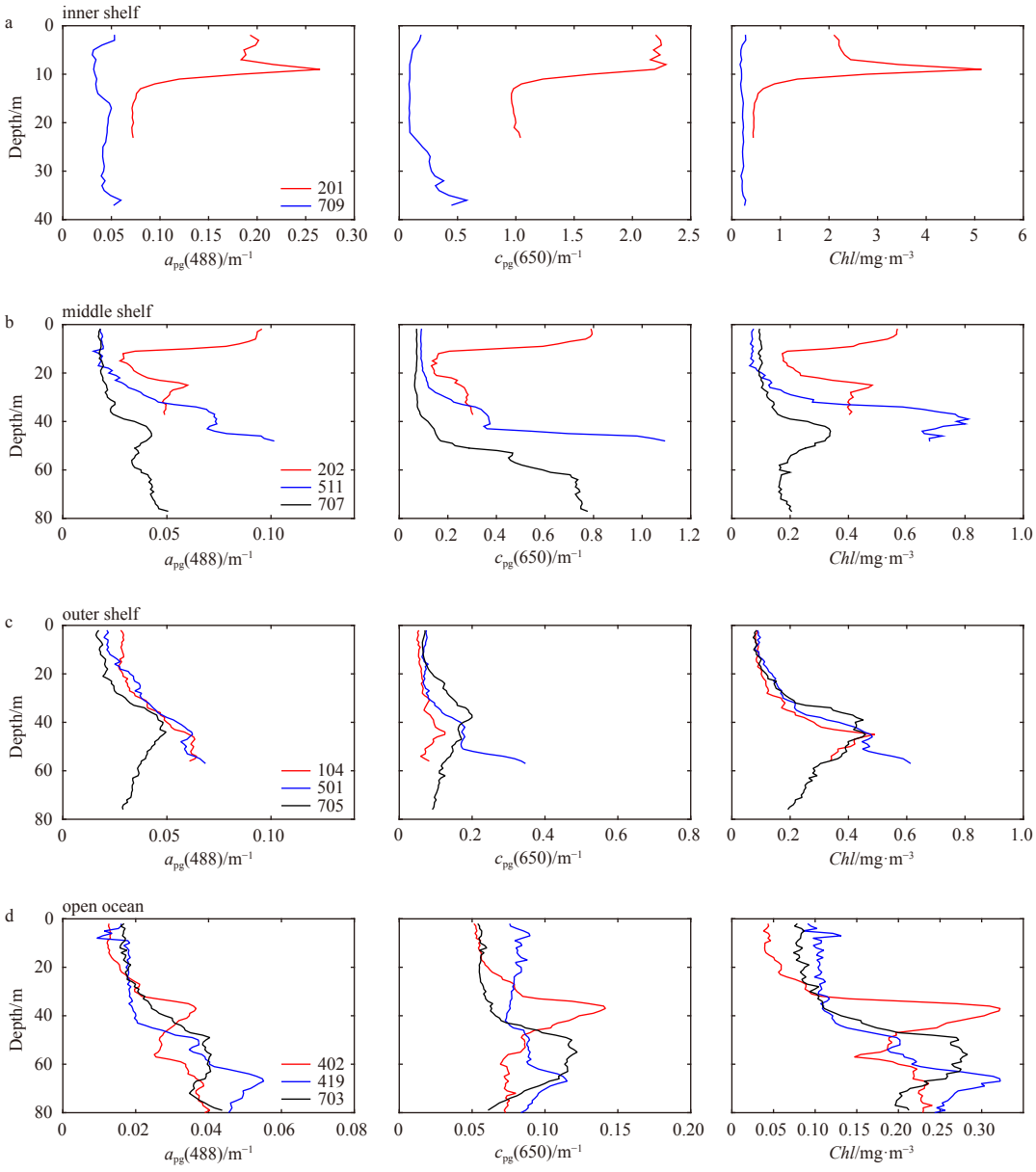

Fig. 7. Typical vertical distributions of non-water absorption coefficient at 488 nm ($a_{pg}(488)$, m^{-1}), non-water attenuation coefficient at 650 nm ($c_{pg}(650)$, m^{-1}) and absorption-estimated *Chl* (mg/m^3)) at stations across the shelf of the NSCS: Inner Shelf (a), Middle Shelf (b), Outer Shelf (c), and Open Ocean (d).

4.24 mg/m^2 and 13.77 mg/m^2, consistent with the very oligotrophic status of open ocean waters in the NSCS. Several typical profiles from the CTD casts were selected to describe regional differences in the vertical distributions of IOPs (Figs 6d and 7d). At Sta. 402, the depth of maximum IOPs is around 37 m, which is consistent with a shoaling of the mixed layer. In the vertical profile of IOPs at Sta. 703, which is representative of profiles in the open ocean, Z_{SCM} is around 56 m. Station 419 lies near the center of a warm eddy (Fig. 1). The water column at Sta. 419 is characterized by warmer and low salinity water in the upper ocean, with the mixed layer being around 50 m and the deep SCML being around 69 m. As demonstrated by the typical profiles, vertical plots of $Chl/c_{pg}(650)$ in open oceanic waters exhibit less variability within the mixed layer, and this variability tends to increase with depth to the bottom of the euphotic zone (Fig. 8d).

3.3 *Variations in the subsurface maximum layer of phytoplankton*

Subsurface maximum layers of phytoplankton were generally observed in most offshore regions of the South China Sea. Based on the estimated profiles of *Chl* from middle shelf waters to open ocean, Z_{SCM} was found to vary from 25 m to 84 m, with the magnitude of SCM between 0.184 mg/m^3 and 0.811 mg/m^3. For most stations, variations in Z_{SCM} followed fluctuations of the isopycnal, σ_θ=23 kg/m^3, and the isotherm, θ=23.38°C (Figs 9a, b). However, there are two abnormal stations that exhibit large deviations between Z_{SCM} and the isopycnal, σ_θ=23 kg/m^3. One is Sta. 402 (21°N, 120°E), located to the southwest of Taiwan Island, near the Luzon Strait (Fig. 1), where Z_{SCM} and the depth of the isopycnal (σ_θ=23 kg/m^3) are at 37 m and 119 m, respectively. As illustrated in the θ-S relationship, this area could be influenced by an intrusion of water from the Kuroshio Current through the Luzon Strait, as suggested by higher subsurface salinity and temperat-

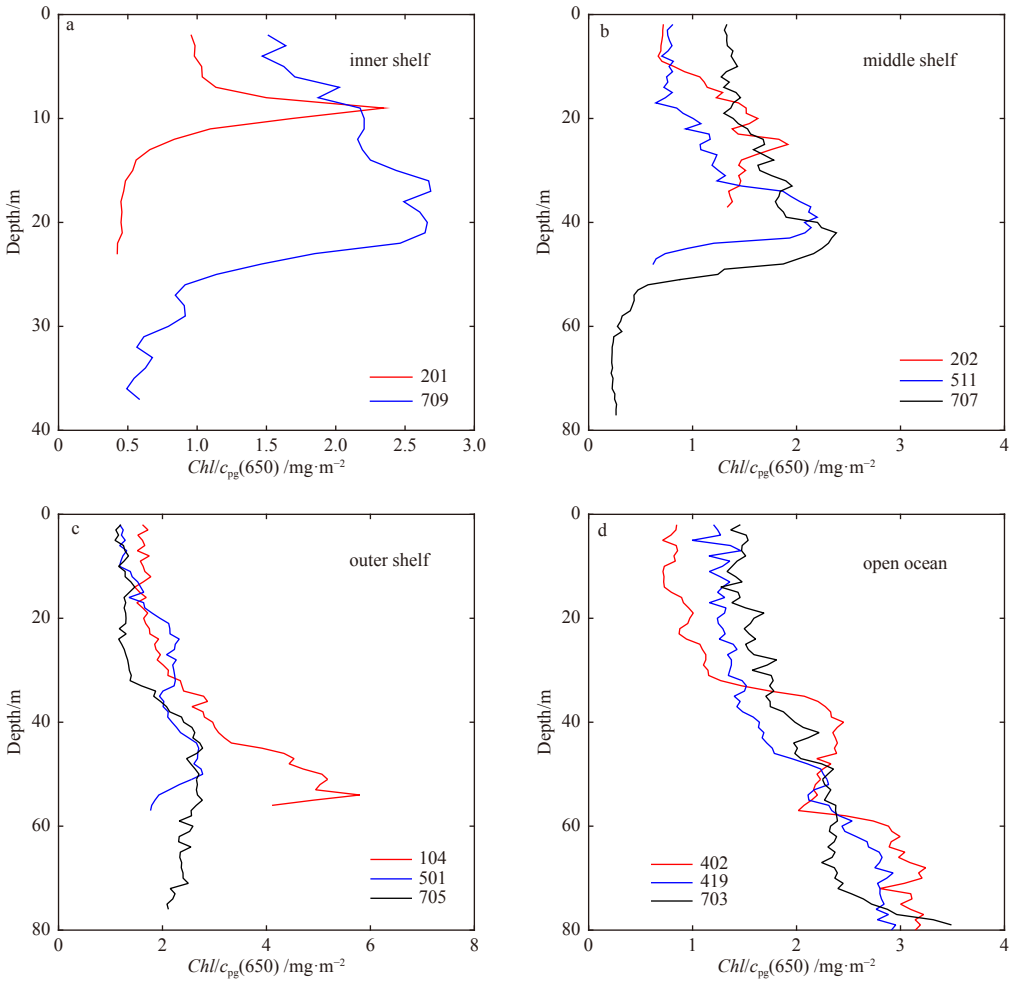

Fig. 8. Typical vertical distributions of the $Chl/c_{pg}(650)$ (mg/m^2) at stations across the shelf of the NSCS: inner shelf (a), middle shelf (b), outer shelf (c), and open ocean (d).

ure in the upper water column. Another abnormal station is 609, located in the central part of NSCS, with Z_{SCM} and depth of the isopycnal (σ_θ=23 kg/m^3) at 43 m and 83 m, respectively. This station was observed after the passage of typhoon Nuri (Ye et al., 2013). In both abnormal stations, the vertical hydrological properties showed unique structures with shallow density surface rising toward the surface, and the deep density surface dipping downward. These vertical structures are similar with the mode-eddy reported by McGillicuddy et al. (1999) and McGillicuddy (2016), which is composed of a lens-shaped disturbance that raises the seasonal pycnocline and lowers the main pycnocline.

Excluding these two anomalous stations, Z_{SCM} varies consistently with the depth of isopycnal (σ_θ=23 kg/m^3) and the isotherm (θ=23.38°C), as shown in Figs 9a and b, with the determination coefficients (R^2) for linear regression being 0.76 and 0.74, respectively. The magnitude of SCM (Chl_{max}) in the open ocean was much lower than that in the shelf waters. With the deepening of the SCML, Chl_{max} exhibits a decreasing trend (Fig. 9c). The thickness of the SCML ranges between 3.8 m and 54 m and exhibits a weak correlation with Z_{SCM} (R^2=0.36, N=38). Z_{SCM} lies primarily between the mixed layer depth and Z_{eu}, and a linear relationship was observed between Z_{SCM} and Z_{eu}, with R^2=0.76 (N=11).

Based on high-resolution *in situ* measurements, the column-integrated biomass over Z_{eu} (<Chla>$_{Zeu}$) could be quantitatively analyzed. The range of <Chla>$_{Zeu}$ is wide, from 4.24 mg/m^2 in the very oligotrophic waters to 30.34 mg/m^2 at the coastal upwelling station to the east of Guangdong Province. Large scatters were observed for the relationship <Chla>$_{Zeu}$ and Chl_{surf}, especially for open oceanic waters (Fig. 10a). With a deepening of the SCML, the <Chla>$_{Zeu}$ tended to decease, exhibiting a much closer power law relationship with depth, and R^2 reached a maximum of 0.73 (Fig. 10b). A close relationship between <Chla>$_{Zeu}$ and the ratio of Z_{SCM} and Z_{eu} (Z_{SCM}/Z_{eu}) was also observed, with an R^2 of 0.72 (Fig. 10c).

4 Discussion

4.1 *Physical processes influencing the profiles of bio-optical properties*

Bulk variabilities of absorption and attenuation coefficients with *Chl* and POC are consistent with previous studies in the SCS, which indicate the importance of phytoplankton and its accompanying materials (Wang et al., 2008; Cui et al., 2016). Physical processes play an important role in determining the spatial variations observed in our profiles of bio-optical properties in the NSCS. Coastal upwelling and river discharge are two important features of the inner and middle shelf waters of the NSCS, which supply nutrients that support phytoplankton growth by Ekman pumping and freshwater discharge, respectively. These results are consistent with previous studies in NSCS (Lu et al., 2010; Lin

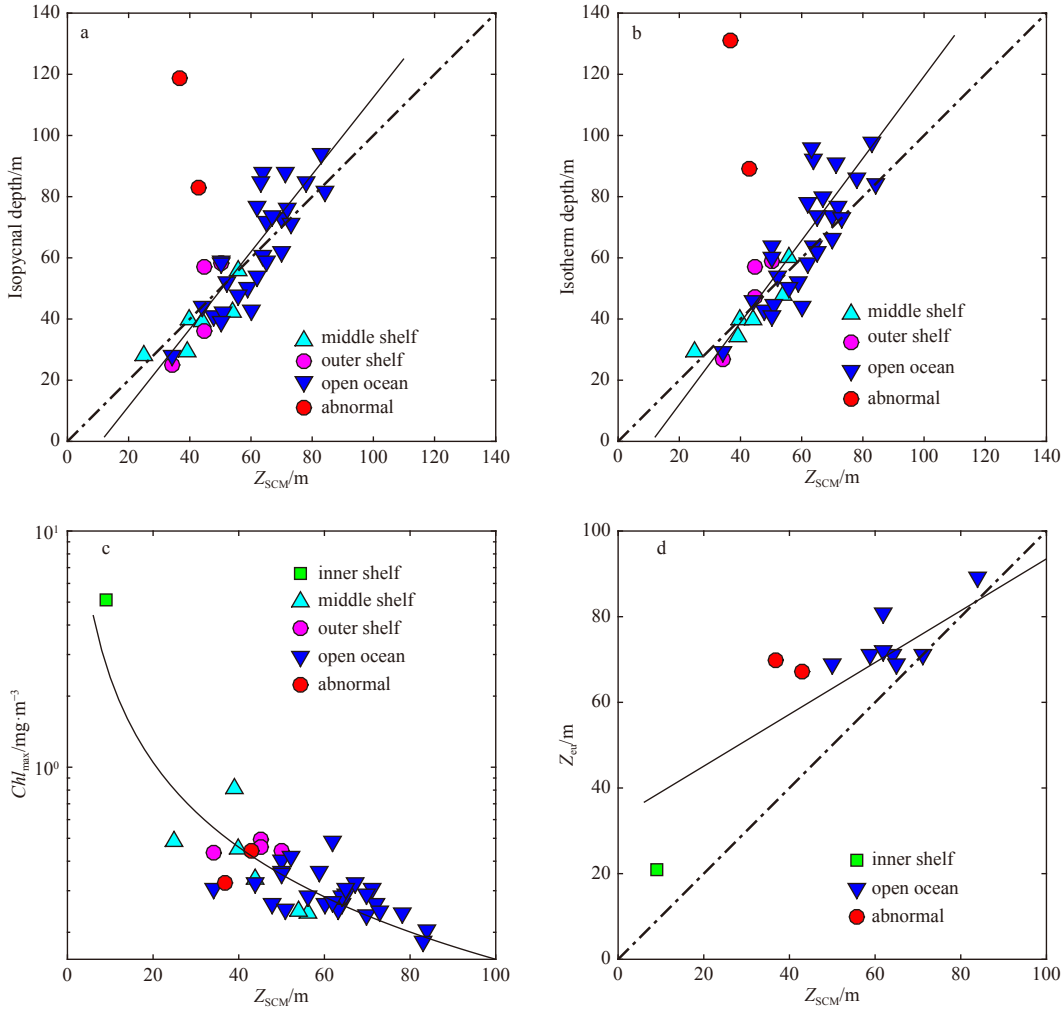

Fig. 9. Scatterplots of the depth of the SCML (Z_{SCM}) as function of the isopycnal depth at σ_θ=23 kg/m^3 (a), the isotherm depth at θ=23.38°C (b), the magnitude of SCM (Chl_{max}) (c), and depth to the bottom of the euphotic zone (Z_{eu}) (d). Colors/markers refer to the different sub-regions. The line corresponds to the linear (a, b, d) or power-law (c) fit function.

et al., 2014; Xu et al., 2018). Terrestrial material could also been exported from the Zhujiang River plume or the upwelling process which resulted higher attenuation coefficient (c_{pg}(650)) in the upper layer of inner shelf water (Cui et al., 2016). Conspicuous shoaling of the isotherms from the middle shelf to the inner shelf in coastal upwelling areas could induce resuspension of particles and the transport of detrital matter within the bottom boundary layer. This process would be consistent with the high attenuation coefficients observed below the SCML that increased rapidly towards the bottom, as well as the decreasing trend of Chl/c_{pg}(650) in the middle and outer shelf waters. Similar characteristics of attenuation coefficient profiles have been investigated in the bottom boundary layer of a continental shelf in the Mid-Atlantic Bight (Boss et al., 2001). These patterns observed in bio-optical properties are consistent with the summertime hydrography and nutrient dynamics of the NSCS as discussed by Wong et al. (2015). Vertical mixing within the NSCS shelf-sea area is the primary mechanism for bringing nutrients from the sub-surface of the adjoining ocean basin up to the mixed layer of the shelf, supporting primary production. Based on our survey data, coastal upwelling was found to be the primary mechanism contributing to vertical mixing in northeast and northwest part of the NSCS (Lin et al., 2014).

In the open ocean area, phytoplankton was the dominant factor influencing the vertical distribution of bio-optical properties (Figs 2 and 7d). The subsurface maximum of the a_{pg}(488) and c_{pg}(650) were corresponding to the subsurface maximum of *Chl*. Cui et al. (2016) has ever reported similar variability in the shelf and basin waters in the NSCS during summer. However, this is different from the vertical separation of the maxima of biomass (as reflected by c_p) and chlorophyll during stratified conditions observed in some oligotrophic system (e.g., Sta. ALOHA in the subtropical North Pacific Ocean), caused by algal photo-adaptation (Fennel and Boss, 2003 and references therein). The SCML is a nearly ubiquitous feature in stably stratified waters, and the depth of the SCML is found to be consistent with the top of the nitracline where phytoplankton growth is enhanced by the optimal combination of nutrient flux and irradiance (Cullen, 2015). In our study area, a combination of mesoscale eddies, intrusions of Kuroshio water, and occasional typhoons are responsible for the variability of the SCML in the open ocean observed during the survey period. A clear relationship was observed between the depth of the SCML (Z_{SCM}) and the fluctuation of thermocline depth as denoted by the isopycnal (σ_θ=23 kg/m^3) and the iso-

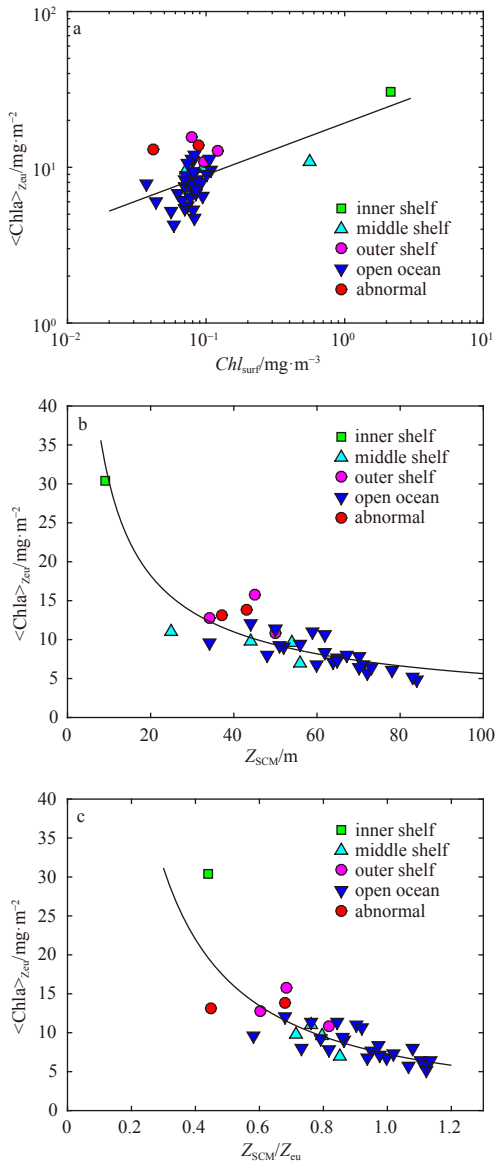

Fig. 10. Scatterplots of the column-integrated biomass over Z_{eu} (<Chla>$_{Zeu}$) as a function of Chl_{surf} (a), Z_{SCM} (b), and Z_{SCM}/Z_{eu} (c). Solid lines indicate the power-law fit function. Colors/markers refer to different sub-regions.

therm at 23.38°C. This observation confirms the importance of physical forcing on regulating the SCML within the euphotic zone (Wong et al., 2015). These results were also consistent with those reported in previous studies of the NSCS, which indicated that the vertical distribution of nutrients generally follows isopycnal (and largely isothermal) surfaces in the upper water column (Chen et al., 2006; Li et al., 2016; Zhang et al., 2016). These effects could be easily explained based on the doming of the isopycnals and the nutricline, where nutrient pumping may have been caused by a cold eddy, or by the passage of typhoon Nuri (McGillicuddy et al., 1999; McGillicuddy, 2016; Ye et al., 2013; Xu et al., 2018). However, the relationship may not hold true for specific profiles with complex hydrological structure, for example, at Stas 402 and 609. A clear uplift of the SCM was observed at both stations, however, the isopycnal depth (σ_θ=23 kg/m^3) relatively deeper than nearby stations. These phenomena might be related with the unique hydrological profiles caused by intrusion of Kuroshio waters or by the passage of typhoon Nuri, respectively. Shoaling density surfaces may lift nutrients into the euphotic zone, which are rapidly utilized by the biota, and the subsurface maximum layer of chlorophyll (SCML) could be lifted up (McGillicuddy et al., 1999; McGillicuddy, 2016). However, deepening density surface serve to push nutrient-depleted water out of the well-illuminated surface layers, which may result in the departures from general relationship between Z_{SCM} and the ispycnal at 23 kg/m^3 (as well as the isotherm at 23.38°C). Driving mechanisms may be even more complicated in the case of anticyclonic eddies (ACEs) (Wang et al., 2018). Based on our observations, for those profiles located in the two ACEs across the 18°N transact, the SCML lies mainly between 64–84 m, with Z_{SCM} generally following the depth patterns of the isopycnals (Figs 9a, b). Since the optical instrument (ac9) was mainly deployed to depths <90 m, there were also some profiles where the SCML was too deep to be detected. Full-depth observations and additional studies are expected in future work.

Based on *in situ* measured data with high vertical resolution, a more accurate assessment of *Chl* integrated over the whole water column of the euphotic zone could be achieved to investigate ecological responses to different physical processes. Although a general trend could be detected from surface *Chl* concentrations, which showed that the total biomass within the euphotic zone decreases from the coastal ocean to open oceanic waters, it is difficult to estimate the total chlorophyll *a* inventory of the surface phytoplankton biomass for those oligotrophic waters in the open ocean of the SCS (Fig. 10a). This may introduce a large uncertainty in the estimation of primary production from ocean color, since only the pigment content within the upper penetration depth is accessible to remote sensing techniques. The relationship between <Chla>$_{Zeu}$ and surface *Chl* is different from that developed for stratified waters in open ocean (Morel et al., 2001; Uitz et al., 2006). With deepening of the SCML, <Chla>$_{Zeu}$ tends to decease, exhibiting a much closer power law relationship. This variability is consistent with that observed by Mignot et al. (2011), confirming that the upward flux of nutrients driven by physical processes contributes to phytoplankton growth within the euphotic zone. The magnitude (that is the intensity) of the SCM (Chl_{max}) is sensitive to changes in the depth of the SCML and tends to decrease with deepening of the SCML. Similar results have been reported in previous studies, where they were attributed to nitrate transport from nitrate-rich waters to the euphotic zone (Chen et al., 2006; Mignot et al., 2011; Gong et al., 2015).

4.2 *The effect of light attenuation on the chlorophyll profile*

Light attenuation could be another factor determining the vertical variability of phytoplankton. Previous studies have proposed that both the intensity and the location of the SCML is the result of a balance between the upward flux of nutrients and the downward attenuation of light (Fennel and Boss, 2003; Cullen, 2015). Considering the seasonal variability of the SCML, light attenuation could be a critical factor in regulating the depth of the SCML, as discussed by Gong et al. (2015) based on physical-biogeochemical modelling and by Mignot et al. (2011) based on *in situ* observed profiles. During our survey period, the euphotic zone depth (Z_{eu}) was generally deeper than the mixed layer depth. Light was therefore readily available and likely not a limiting factor of phytoplankton growth in the mixed layer. Z_{SCM} lies primarily between the mixed layer depth and Z_{eu}, and a close relationship between Z_{SCM} and Z_{eu} was observed with R^2=0.76 (N=11). Due to the limit of *in situ* observations of underwater

light field, the relationship between Z_{SCM} and Z_{eu} (Fig. 9d) could be improved in future. For waters with low *Chl* in the upper layer, the SCML deepens and becomes closer to the nitracline, which may reduce the phytoplankton biomass at the SCML. Light attenuation in the upper water column is the primary factor affecting vertical variations in phytoplankton growth rates (Mignot et al., 2011, 2014; Gong et al., 2014, 2015). The relative positions of the SCML and the euphotic zone depth may result in variability of total integrated phytoplankton biomass within Z_{eu} (Fig. 10c). Since the distribution of the SCML depth was primarily regulated by fluctuations in the thermocline, this relationship reflects the combined effect of physical forcing and light attenuation to phytoplankton growth in our study area.

Vertical profiles of $Chl/c_{pg}(650)$ in the open ocean of the NSCS show similar patterns with vertical distributions of the *Chl*:C ratio observed in California Current pelagic ecosystem (Li et al., 2010). These patterns reveal the great advantage of optical measurements in quantifying phytoplankton dynamics in the ocean. Cui et al. (2016) also found similar correlations between $c_p(660)$ and POC for data collected in the NSCS, with the exception of nearshore stations with high sediment resuspension. The $Chl/c_{pg}(650)$ ratio is low at the sea surface as a result of the strong light intensity compared with deeper layers, and tends to increase with depth as a result of photoadaptation (Behrenfeld et al., 2005; Xing et al., 2014), exhibiting relatively constant values near the bottom of the euphotic zone. This is a common feature of open ocean waters characterized by strong stratification (e.g., Kitchen and Zaneveld, 1990; Fennel and Boss, 2003) and has been attributed to complex interactions between light, nutrients, temperature, and phytoplankton community structures (Li et al., 2010; Nencioli et al., 2010).

5 Conclusions

We studied the vertical distribution of bio-optical properties based on high-resolution profiles of absorption and attenuation in the NSCS during summer 2008. *Chl* profiles were estimated from the differences in absorption in the red wavelengths, which gave us detailed information about the vertical variability of phytoplankton in the NSCS, as well as the column-integrated biomass over the euphotic depth.

Vertical distributions of both IOPs and the estimated *Chl* in the NSCS exhibit significant differences across the continental shelf and between the shelf and open ocean. Physical processes including coastal upwelling and discharge from the Zhujiang River were found to be the main drivers controlling bio-optical properties in inner shelf waters, by supplying nutrients to the upper water column that support phytoplankton growth, and by transporting detritus along the bottom boundary layer. Profiles of IOPs and *Chl* in inner shelf stations were characterized by relatively high values at the surface and at the bottom, with or without a SCML. In the middle shelf and some of the outer-shelf stations, the attenuation coefficients below the SCML are high and tend to increase rapidly towards the bottom. This is a distinguishing characteristic that is consistent with the transport of colder and relatively nutrient-rich water from the open ocean to the shelf-sea along the bottom of the ocean, with the additional influence of resuspended particulate matter over the bottom boundary layer. For open ocean waters, vertical profiles of IOPs and *Chl* are much more similar, with the depth of their maximum values ranging from 34 m to 84 m with some stations even deeper. A combination of physical processes including mesoscale eddies, Kuroshio intrusions, and typhoons caused variability in the depth and thickness of the SCML in the open ocean during the survey period. The depth of Z_{SCM} varies consistently with fluctuations in the isopycnal (σ_θ=23 kg/m^3) and the isotherm (θ=23.38°C), which are primarily caused by meso-scale eddies. However, for waters affected by Kuroshio intrusions and typhoons, Z_{SCM} exhibits a significant displacement relative to the isolines of temperature and density due to unique hydrological structures with shallow density surface rising toward the surface, and the deep density surface dipping downward. Light attenuation was another important factor influencing the vertical structure of phytoplankton by regulating the depth of the SCML and the $Chl/c_{pg}(650)$ distribution. The column-integrated biomass over Z_{eu} ($<Chla>_{Zeu}$) exhibited a large scatter in offshore oligotrophic waters with low surface chlorophyll. Fluctuations in the depth of the SCML, especially the position of the SCML relative to that of Z_{eu}, played an important role in determining the variability of $<Chla>_{Zeu}$, confirming the combined effects of physical forcing and light attenuation on phytoplankton growth in NSCS.

Our observations of the vertical variations of phytoplankton provide much more detailed information about the marine ecological dynamics of the NSCS, with great improvements over data based on conventional bottle-sampling methods. With the advancement of bio-optical monitoring instruments, further intensive research can be conducted to study the vertical variability of phytoplankton biomass and associated carbon fluxes, as well as important driving factors over different spatial and temporal scales.

Acknowledgements

We thank all contributors to the dataset in the South China Sea Open Cruise by the R/V *Shiyan 3*, South China Sea Institute of Oceanology, CAS and Qian Li for his constructive suggestions on the initial version of the manuscript. We also thank Guy Evans from Liwen Bianji, Edanz Editing China (www.liwenbianji.cn/ac), for editing the English text of a draft of this manuscript.

References

Barnard A H, Pegau W S, Zaneveld J R V. 1998. Global relationships of the inherent optical properties of the oceans. Journal of Geophysical Research, 103(C11): 24955–24968, doi: 10.1029/98JC01851

Behrenfeld M J, Boss E. 2003. The beam attenuation to chlorophyll ratio: an optical index of phytoplankton physiology in the surface ocean?. Deep Sea Research Part I: Oceanographic Research Papers, 50(12): 1537–1549, doi: 10.1016/j.dsr.2003.09.002

Behrenfeld M J, Boss E, Siegel D A, et al. 2005. Carbon-based ocean productivity and phytoplankton physiology from space. Global Biogeochemical Cycles, 19(1): GB1006

Bishop J K B. 1999. Transmissometer measurement of POC. Deep Sea Research Part I: Oceanographic Research Papers, 46(2): 353–369, doi: 10.1016/S0967-0637(98)00069-7

Boss E S, Collier R, Larson G, et al. 2007. Measurements of spectral optical properties and their relation to biogeochemical variables and processes in Crater Lake, Crater Lake National Park, OR. Hydrobiologia, 574(1): 149–159, doi: 10.1007/s10750-006-2609-3

Boss E, Pegau W S, Gardner W D, et al. 2001. Spectral particulate attenuation and particle size distribution in the bottom boundary layer of a continental shelf. Journal of Geophysical Research: Oceans, 106(C5): 9509–9516, doi: 10.1029/2000JC900077

Boss E, Picheral M, Leeuw T, et al. 2013. The characteristics of particulate absorption, scattering and attenuation coefficients in the surface ocean; Contribution of the Tara Oceans expedition. Methods in Oceanography, 7: 52–62, doi: 10.1016/j.mio.2013.11.002

Brewin R J W, Dall'Olmo G, Pardo S, et al. 2016. Underway spectrophotometry along the Atlantic Meridional Transect reveals high

performance in satellite chlorophyll retrievals. Remote Sensing of Environment, 183: 82–97, doi: 10.1016/j.rse.2016.05.005
Buesseler K O. 2001. Ocean biogeochemistry and the global carbon cycle: an introduction to the U.S. joint global ocean flux study. Oceanography, 14(4): 5, doi: 10.5670/oceanog.2001.01
Chang G C, Dickey T D. 2001. Optical and physical variability on timescales from minutes to the seasonal cycle on the New England shelf: July 1996 to June 1997. Journal of Geophysical Research: Oceans, 106(C5): 9435–9453, doi: 10.1029/2000JC900069
Chen C C, Shiah F K, Chung S W, et al. 2006. Winter phytoplankton blooms in the shallow mixed layer of the South China Sea enhanced by upwelling. Journal of Marine Systems, 59(1–2): 97–110, doi: 10.1016/j.jmarsys.2005.09.002
Claustre H, Fell F, Oubelkheir K, et al. 2000. Continuous monitoring of surface optical properties across a geostrophic front: Biogeochemical inferences. Limnology and Oceanography, 45(2): 309–321
Cui Wansong, Wang Difeng, Gong Fang, et al. 2016. The vertical distribution of the beam attenuation coefficient and its correlation to the particulate organic carbon in the north South China Sea. In: Remote Sensing of the Ocean, Sea Ice, Coastal Waters, and Large Water Regions. Edinburgh, United Kingdom: SPIE, 2016
Cullen J J. 1982. The deep chlorophyll maximum: Comparing vertical profiles of chlorophyll *a*. Canadian Journal of Fisheries and Aquatic Sciences, 39(5): 791–803, doi: 10.1139/f82-108
Cullen J J. 2015. Subsurface chlorophyll maximum layers: Enduring enigma or mystery solved?. Annual Review of Marine Science, 7: 207–239, doi: 10.1146/annurev-marine-010213-135111
Dickey T D. 2001. The role of new technology in advancing ocean biogeochemical research. Oceanography, 14(4): 108–120, doi: 10.5670/oceanog.2001.11
Fennel K, Boss E. 2003. Subsurface maxima of phytoplankton and chlorophyll: Steady-state solutions from a simple model. Limnology and Oceanography, 48(4): 1521–1534, doi: 10.4319/lo.2003.48.4.1521
Fujii M, Boss E, Chai F. 2007. The value of adding optics to ecosystem models: a case study. Biogeosciences, 4(5): 817–835, doi: 10.5194/bg-4-817-2007
Gardner W D, Gundersen J S, Richardson M J, et al. 1999. The role of seasonal and diel changes in mixed-layer depth on carbon and chlorophyll distributions in the Arabian Sea. Deep Sea Research Part II: Topical Studies in Oceanography, 46(8–9): 1833–1858, doi: 10.1016/S0967-0645(99)00046-6
Gernez P, Antoine D, Huot Y. 2011. Diel cycles of the particulate beam attenuation coefficient under varying trophic conditions in the northwestern Mediterranean Sea: Observations and modeling. Limnology and Oceanography, 56(1): 17–36, doi: 10.4319/lo.2011.56.1.0017
Gong Xiang, Shi Jie, Gao Huiwang, et al. 2014. Modeling seasonal variations of subsurface chlorophyll maximum in South China Sea. Journal of Ocean University of China, 13(4): 561–571, doi: 10.1007/s11802-014-2060-4
Gong Xiang, Shi Jinhui, Gao Huiwang, et al. 2015. Steady-state solutions for subsurface chlorophyll maximum in stratified water columns with a bell-shaped vertical profile of chlorophyll. Biogeosciences, 12(4): 905–919, doi: 10.5194/bg-12-905-2015
Kara A B, Rochford P A, Hurlburt H E. 2000. An optimal definition for ocean mixed layer depth. Journal of Geophysical Research, 105(C7): 16803–16821, doi: 10.1029/2000JC900072
Kheireddine M, Antoine D. 2014. Diel variability of the beam attenuation and backscattering coefficients in the northwestern Mediterranean Sea (BOUSSOLE site). Journal of Geophysical Research: Oceans, 119(8): 5465–5482, doi: 10.1002/2014JC010007
Kitchen J C, Zaneveld J R V. 1990. On the noncorrelation of the vertical structure of light scattering and chlorophyll α in case I waters. Journal of Geophysical Research: Oceans, 95(C11): 20237–20246, doi: 10.1029/JC095iC11p20237
Knap A, Michaels A, Close A, et al. 1996. Protocols for the Joint Global Ocean Flux Study (JGOFS) core measurements. Reprint of the IOC Manuals and Guides No. 29, UNESCO, Paris
Lavigne H, D'Ortenzio F, D'Alcalà M R, et al. 2015. On the vertical distribution of the chlorophyll *a* concentration in the Mediterranean Sea: a basin-scale and seasonal approach. Biogeosciences, 12(16): 5021–5039, doi: 10.5194/bg-12-5021-2015
Li Q P, Dong Y, Wang Y. 2016. Phytoplankton dynamics driven by vertical nutrient fluxes during the spring inter-monsoon period in the northeastern South China Sea. Biogeosciences, 13: 455–466, doi: 10.5194/bg-13-455-2016
Li Q P, Franks P J S, Landry M R, et al. 2010. Modeling phytoplankton growth rates and chlorophyll to carbon ratios in California coastal and pelagic ecosystems. Journal of Geophysical Research, 115(G4): G04003
Lin Junfang, Cao Wenxin, Wang Guifen, et al. 2014. Inversion of bio-optical properties in the coastal upwelling waters of the northern South China Sea. Continental Shelf Research, 85: 73–84, doi: 10.1016/j.csr.2014.06.001
Lin Peigen, Cheng Peng, Gan Jianping, et al. 2016. Dynamics of wind-driven upwelling off the northeastern coast of Hainan Island. Journal of Geophysical Research: Oceans, 121(2): 1160–1173, doi: 10.1002/2015JC011000
Liu K K, Chao S Y, Shaw P T, et al. 2002. Monsoon-forced chlorophyll distribution and primary production in the South China Sea: observations and a numerical study. Deep Sea Research Part I: Oceanographic Research Papers, 49(8): 1387–1412, doi: 10.1016/S0967-0637(02)00035-3
Liu Fenfen, Tang Shilin, Chen Chuqun. 2013. Impact of nonlinear mesoscale eddy on phytoplankton distribution in the northern South China Sea. Journal of Marine Systems, 123–124: 33–40, doi: 10.1016/j.jmarsys.2013.04.005
Lu Zhongming, Gan Jianping, Dai Minhan, et al. 2010. The influence of coastal upwelling and a river plume on the subsurface chlorophyll maximum over the shelf of the northeastern South China Sea. Journal of Marine Systems, 82(1–2): 35–46, doi: 10.1016/j.jmarsys.2010.03.002
Ma Jinfeng, Zhan Haigang, Du Yan. 2011. Seasonal and interannual variability of surface CDOM in the South China Sea associated with El Niño. Journal of Marine Systems, 85(3–4): 86–95, doi: 10.1016/j.jmarsys.2010.12.006
McGillicuddy D J Jr. 2016. Mechanisms of physical-biological-biogeochemical interaction at the oceanic mesoscale. Annual Review of Marine Science, 8(1): 125–159, doi: 10.1146/annurev-marine-010814-015606
McGillicuddy D J Jr, Johnson R, Siegel D A, et al. 1999. Mesoscale variations of biogeochemical properties in the Sargasso Sea. Journal of Geophysical Research: Oceans, 104(C6): 13381–13394, doi: 10.1029/1999JC900021
Mignot A, Claustre H, D'Ortenzio F, et al. 2011. From the shape of the vertical profile of in vivo fluorescence to Chlorophyll-*a* concentration. Biogeosciences, 8(8): 2391–2406, doi: 10.5194/bg-8-2391-2011
Mignot A, Claustre H, Uitz J, et al. 2014. Understanding the seasonal dynamics of phytoplankton biomass and the deep chlorophyll maximum in oligotrophic environments: A Bio-Argo float investigation. Global Biogeochemical Cycles, 28(8): 856–876, doi: 10.1002/2013GB004781
Mitchell B G, Kahru M, Wieland J, et al. 2003. Determination of spectral absorption coefficients of particles, dissolved material and phytoplankton for discrete water samples. In: Mueller J L, Fargoin G S, McClain C R, eds. Ocean Optics Protocols for Satellite Ocean Color Sensor Validation, revision 4, Vol. IV (Chapter 4), NASA/TM-2003-211621/Rev4-vol. 4. Greenbelt, MD: NASA Goddard Space Flight Center, 39–64
Mobley C D. 1994. Light and Water: Radiative Transfer in Natural Waters. San Diego, CA, USA: Academic Press
Morel A. 1988. Optical modeling of the upper ocean in relation to its biogenous matter content (case I waters). Journal of Geophysical Research: Oceans, 93(C9): 10749–10768, doi: 10.1029/JC093iC09p10749
Morel A, Maritorena S. 2001. Bio-optical properties of oceanic waters: A reappraisal. Journal of Geophysical Research: Oceans,

106(C4): 7163–7180, doi: 10.1029/2000JC000319
Nencioli F, Chang G, Twardowski M, et al. 2010. Optical characterization of an eddy-induced diatom bloom west of the island of Hawaii. Biogeosciences, 7(1): 151–162, doi: 10.5194/bg-7-151-2010
Ning Xiuren, Chai Fei, Xue Huijie, et al. 2004. Physical-biological oceanographic couplinginfluencing phytoplankton and primary production in the South China Sea. Journal of Geophysical Research: Oceans, 109: C10005, doi: 10.1029/2004JC002365
Oubelkheir K, Claustre H, Sciandra A, et al. 2005. Bio-optical and biogeochemical properties of different trophic regimes in oceanic waters. Limnology and Oceanography, 50(6): 1795–1809, doi: 10.4319/lo.2005.50.6.1795
Oubelkheir K, Sciandra A. 2008. Diel variations in particle stocks in the oligotrophic waters of the Ionian Sea (Mediterranean). Journal of Marine Systems, 74(1–2): 364–371, doi: 10.1016/j.jmarsys.2008.02.008
Pan Xiaoju, Wong G T F, Tai J H, et al. 2015. Climatology of physical hydrographic and biological characteristics of the Northern South China Sea Shelf-sea (NoSoCS) and adjacent waters: Observations from satellite remote sensing. Deep Sea Research Part II: Topical Studies in Oceanography, 117: 10–22, doi: 10.1016/j.dsr2.2015.02.022
Parsons T, Takahashi M, Hargrave B. 1984. Biological Oceanographic Processes. 3rd ed. England: Pergamon Press, 330
Pérez V, Fernández E, Marañón E, et al. 2006. Vertical distribution of phytoplankton biomass, production and growth in the Atlantic subtropical gyres. Deep Sea Research Part I: Oceanographic Research Papers, 53(10): 1616–1634, doi: 10.1016/j.dsr.2006.07.008
Platt T, Bouman H, Devred E, et al. 2005. Physical forcing and phytoplankton distributions. Scientia Marina, 69(S1): 55–73, doi: 10.3989/scimar.2005.69s155
Roesler C S, Barnard A H. 2013. Optical proxy for phytoplankton biomass in the absence of photophysiology: Rethinking the absorption line height. Methods in Oceanography, 7: 79–94, doi: 10.1016/j.mio.2013.12.003
Shang Shaoling, Li Li, Li Jun, et al. 2012. Phytoplankton bloom during the northeast monsoon in the Luzon Strait bordering the Kuroshio. Remote Sensing of Environment, 124: 38–48, doi: 10.1016/j.rse.2012.04.022
Stramski D, Reynolds R A, Babin M, et al. 2008. Relationships between the surface concentration of particulate organic carbon and optical properties in the eastern South Pacific and eastern Atlantic Oceans. Biogeosciences, 5(1): 171–201, doi: 10.5194/bg-5-171-2008
Sullivan J M, Twardowski M S, Zaneveld J R V, et al. 2006. Hyperspectral temperature and salt dependencies of absorption by water and heavy water in the 400–750 nm spectral range. Applied Optics, 45(21): 5294–5309, doi: 10.1364/AO.45.005294
Uitz J, Claustre H, Morel A, et al. 2006. Vertical distribution of phytoplankton communities in open ocean: An assessment based on surface chlorophyll. Journal of Geophysical Research: Oceans, 111(C8): C08005
Wang Guifen, Cao Wenxi, Yang Dingtian, et al. 2008. Variation in downwelling diffuse attenuation coefficient in the northern South China Sea. Chinese Journal of Oceanology and Limnology, 26(3): 323–333, doi: 10.1007/s00343-008-0323-x
Wang Lei, Huang Bangqin, Chiang K P, et al. 2016. Physical-biological coupling in the western South China Sea: The response of phytoplankton community to a mesoscale cyclonic eddy. PLoS One, 11(4): e0153735, doi: 10.1371/journal.pone.0153735
Wang Lei, Huang Bangqin, Laws E A, et al. 2018. Anticyclonic eddy edge effects on phytoplankton communities and particle export in the northern South China Sea. Journal of Geophysical Research: Oceans, 123(11): 7632–7650, doi: 10.1029/2017JC013623
Wang Dongxiao, Shu Yeqiang, Xue Huijie, et al. 2014. Relative contributions of local wind and topography to the coastal upwelling intensity in the northern South China Sea. Journal of Geophysical Research: Oceans, 119(4): 2550–2567, doi: 10.1002/2013JC009172
Wang Guifen, Zhou Wen, Cao Wenxi, et al. 2011. Variation of particulate organic carbon and its relationship with bio-optical properties during a phytoplankton bloom in the Pearl River estuary. Marine Pollution Bulletin, 62(9): 1939–1947, doi: 10.1016/j.marpolbul.2011.07.003
Wong G T F, Pan Xiaoju, Li Kuoyuan, et al. 2015. Hydrography and nutrient dynamics in the Northern South China Sea Shelf-sea (NoSoCS). Deep Sea Research Part II: Topical Studies in Oceanography, 117: 23–40, doi: 10.1016/j.dsr2.2015.02.023
Xing Xiaogang, Claustre H, Uitz J, et al. 2014. Seasonal variations of bio-optical properties and their interrelationships observed by Bio-Argo floats in the subpolar North Atlantic. Journal of Geophysical Research: Oceans, 119(10): 7372–7388, doi: 10.1002/2014JC010189
Xiu Peng, Chai Fei. 2014. Connections between physical, optical and biogeochemical processes in the Pacific Ocean. Progress in Oceanography, 122: 30–53, doi: 10.1016/j.pocean.2013.11.008
Xiu Peng, Liu Yuguang, Li Gang, et al. 2009. Deriving depths of deep chlorophyll maximum and water inherent optical properties: A regional model. Continental Shelf Research, 29(19): 2270–2279, doi: 10.1016/j.csr.2009.09.003
Xu Wenlong, Wang Guifen, Zhou Wen, et al. 2018. Vertical variability of chlorophyll a concentration and its responses to hydrodynamic processes in the northeastern South China Sea in summer. Journal of Tropical Oceanography (in Chinese), 37(5): 62–73
Ye H J, Sui Y, Tang D L, et al. 2013. A subsurface chlorophyll a bloom induced by typhoon in the South China Sea. Journal of Marine Systems, 128: 138–145, doi: 10.1016/j.jmarsys.2013.04.010
Zaneveld J R V, Kitchen J C, Moore C C. 1994. Scattering error correction of reflecting-tube absorption meters. In: Ocean Optics XII. Bergen, Norway: SPIE
Zhang Wenzhou, Wang Haili, Chai Fei, et al. 2016. Physical drivers of chlorophyll variability in the open South China Sea. Journal of Geophysical Research: Oceans, 121(9): 7123–7140, doi: 10.1002/2016JC011983